

The Core Structure of Galaxy Clusters from Gravitational Lensing

Liliya L. R. Williams and Julio F. Navarro ¹

Department of Physics and Astronomy
University of Victoria, Victoria, BC V8P 1A1, Canada

and

Matthias Bartelmann

Max-Planck Institut für Astrophysik, Karl-Schwarzschild Strasse 1,
Garching bei München, D-85740 Germany.

ABSTRACT

We examine gravitational lensing constraints on the structure of galaxy clusters and compare them with the results of cosmological N-body simulations of cluster formation in cold dark matter (CDM) dominated universes. We find that cluster core masses, as measured by the observed location of giant tangential arcs, generally exceed those of dark matter halos of similar velocity dispersion. The magnitude of the discrepancy is a strong function of cluster mass. Arc properties in the most massive clusters in the sample (i.e. those with velocity dispersion, $\sigma \sim 1500 - 2000 \text{ km s}^{-1}$) are essentially consistent with the N-body predictions. On the other hand, giant arcs in $\sigma \sim 1000 \text{ km s}^{-1}$ clusters can only be reconciled with CDM cluster halos if their lensing power has been increased substantially by the presence of a massive ($\sim 3 \times 10^{12} h^{-1} M_{\odot}$) central galaxy and of significant substructure. Best agreement is found if the mass of the central galaxy and the effects of substructure are approximately independent of cluster mass. Massive central galaxies with steep inner density profiles are also needed to explain a clear trend observed in our dataset between the radial thickness of giant tangential arcs and the velocity dispersion of the cluster lens. The position and redshift of radial arcs may be used as independent tests of these results, but at present the dataset available is too limited to have a significant impact on these conclusions. Our results depend only weakly on the cosmological model adopted, and suggest that structural parameters of clusters derived from strong lensing studies cannot usefully constrain the values of cosmological parameters.

1. Introduction

The extraordinary lensing power of galaxy systems first put in evidence by the discovery of giant arcs (Lynds & Petrosian 1986, Soucail et al 1987a) provides an invaluable tool for

¹CIAR Scholar and Sloan Fellow

investigating the gravitational potential of galaxy clusters at moderate redshift. For example, early studies of the giant arcs were instrumental in cementing the view that a monolithic dark matter halo dominates the cluster gravitational potential, to which individual galaxies contribute relatively small local perturbations (Soucail et al 1987b). Detailed studies of the location, morphology, and magnification of giant arcs provide further insight into the mass structure within clusters (AbdelSalam et al 1998, Kneib et al 1996).

The most straightforward interpretation of the location of giant tangential arcs is that they occur roughly at the “Einstein radius” of a cluster, allowing accurate estimates of the total projected mass enclosed within the arc if the angular diameter distances to the lensing cluster and to the arc source galaxy can be measured. This method remains to date the most direct estimator of the total mass projected onto the core of a galaxy cluster. Accurate estimates of the core surface mass density within the arc may be used to place strong upper limits on the core radii of isothermal cluster mass models, and early results were puzzling. Narayan, Blandford & Nityananda (1984) noted that the small cores required to explain the properties of giant arcs were at odds with the relatively large core radii derived from X-ray and optical observations. Small, but finite, core radii were also required to account for observations of radial arcs in clusters such as MS2137-23 (Fort et al 1992) and A370 (Smail et al 1995).

A simple explanation for this discrepancy was proposed by Navarro, Frenk & White (1996, hereafter NFW96) on the basis of cosmological N-body simulations of cluster formation. These authors found that isothermal models are in general a poor approximation to the structure of dark halos formed in N-body simulations, and proposed a simple model to describe the structure of dark matter halos. In this model, which we shall refer to as the “NFW” model, the density profile is shallower than a singular isothermal sphere near the center, and steepens gradually outwards to become steeper than isothermal far from the center. This result explains naturally why models based on the isothermal sphere fail to account simultaneously for lensing and X-ray observations. X-ray core radii, which correspond to the radius where the *local slope* of the mass profile is close to the isothermal value, occur in NFW halos at different radii than giant arcs, whose location trace the radius where the *average inner surface density* equals the “critical” lensing value (see eq. 9 below).

Subsequent work by Navarro, Frenk & White (1997, hereafter NFW97) showed that the structure of dark halos is approximately independent of mass, power spectrum, and cosmological parameters, and demonstrated how a simple algorithm may be used to calculate the mass profile of halos of arbitrary mass in hierarchical universes. The procedure applies only to halos that are close to dynamical equilibrium and assumes spherical symmetry, but it has no free parameters and can be used to predict the location and magnification of giant tangential arcs (as well as of radial arcs) once the velocity dispersion of the cluster and the angular diameter distances to the source galaxy and the cluster lens are specified. Thus, in principle, lensing observations may be used to test directly the overall applicability of the results of N-body simulations to the structure of dark halos on the scale of galaxy clusters.

In this paper we compile the results of gravitational lensing studies of 24 galaxy clusters to investigate whether the properties of gravitationally lensed arcs are consistent with the NFW dark halo model. We discuss the lensing properties of NFW halos in §2 and summarize the main properties of our dataset in §3. Section 4 presents our main results. In §5 we discuss the implications of our model, and in §6 we summarize our main findings.

2. Lensing Properties of NFW halos

2.1. The NFW mass profile

As discussed by NFW96 and NFW97, the spherically averaged density profiles of equilibrium dark matter halos formed in cosmological N-body simulations of hierarchically clustering universes are well represented by a simple formula,

$$\frac{\rho(r)}{\rho_{crit}} = \frac{\delta_c}{(r/r_s)(1+r/r_s)^2}, \quad (1)$$

where $\rho_{crit} = 3H^2/8\pi G$ is the critical density for closure, $H(z)$ is the Hubble parameter,² δ_c is a dimensionless characteristic density contrast, and r_s is a scale radius. If we define the mass of a halo, M_{200} , as the total mass of a sphere of mean density 200 times critical, eq.(1) above has a single free parameter once the halo mass is specified. (The radius of this sphere, r_{200} , is sometimes called the “virial” radius.) The free parameter can be taken to be the characteristic density contrast δ_c or the “concentration” parameter, $c = r_{200}/r_s$. These two parameters are related by

$$\delta_c = \frac{200}{c} \frac{c^3}{\ln(1+c) - c/(1+c)}. \quad (2)$$

The numerical experiments of NFW97 indicate that δ_c is determined by the mean matter density of the universe at the redshift of collapse of each halo, i.e. $\delta_c(M_{200}) \propto (1 + z_{coll}(M_{200}))^3$. Halos of increasing mass collapse later in hierarchical universes, and therefore δ_c and c are monotonically decreasing functions of M_{200} . Collapse redshifts can be easily calculated once the cosmological model is specified, and NFW97 describe a simple algorithm that can be used to calculate the density profile of halos of arbitrary mass in cold dark matter dominated universes (see the Appendix of NFW97 for details).

2.2. Lensing by NFW halos

The lensing properties of axially symmetric lenses is described in detail in Schneider, Ehlers & Falco (1992) and in the many reviews of gravitational lensing (see, e.g., Blandford & Narayan 1992,

²We parameterize the present value of Hubble’s constant by $H_0 = 100 h \text{ km s}^{-1}\text{Mpc}^{-1}$.

Narayan & Bartelmann 1995). Provided that the gravitational potential causing the deflection is small, $|\Phi| \ll c^2$, the lens equation describing the mapping of the source plane into the image plane is very simple. In terms of the angular diameter distances to the lens (D_l), to the source (D_s), and between lens and source (D_{ls}), a lens is locally described by the Jacobian matrix of the mapping,

$$A = \left(\delta_{ij} - \frac{\partial^2 \psi}{\partial \theta_i \partial \theta_j} \right), \quad (3)$$

where $\vec{\theta} = (\theta_i, \theta_j)$ are angular coordinates relative to the optical axis, and ψ is the projected Newtonian potential of the lens,

$$\psi(\vec{\theta}) = \frac{D_{ls}}{D_l D_s} \frac{2}{c^2} \int_{-\infty}^{+\infty} \Phi(D_l \vec{\theta}, z) dz \quad (4)$$

The lensing properties of NFW halo models are fully specified by the radial dependence of the surface mass density in units of the critical surface mass density Σ_{cr} ; the “convergence”,

$$\kappa(x) = \frac{\Sigma(x)}{\Sigma_{cr}}, \quad (5)$$

where Σ_{cr} depends on the lens-source configuration through

$$\Sigma_{cr} = \frac{c^2}{4\pi G} \frac{D_s}{D_l D_{ls}}, \quad (6)$$

and $x = r/r_s$ is the radius in units of the NFW scale radius. Following the derivation of Bartelmann (1996), the mass inside radius x can be described by the dimensionless function,

$$m(x) = 2 \int_0^x \kappa(y) y dy, \quad (7)$$

which can be used to find the eigenvalues of the Jacobian matrix A ,

$$\lambda_r = 1 - \frac{d}{dx} \frac{m}{x} \quad (8)$$

$$\lambda_t = 1 - \frac{m}{x^2}. \quad (9)$$

The tangential and radial critical curves occur at x_t and x_r , where $\lambda_t = 0$ and $\lambda_r = 0$, respectively. The surface density associated with an NFW model (eq.1) is

$$\Sigma(x) = \frac{2 \delta_c \rho_{crit} r_s}{x^2 - 1} f(x), \quad (10)$$

with

$$f(x) = \begin{cases} 1 - (2/\sqrt{x^2 - 1}) \tan^{-1} \sqrt{(x-1)/(x+1)} & \text{if } x > 1; \\ 1 - (2/\sqrt{1-x^2}) \tanh^{-1} \sqrt{(1-x)/(1+x)} & \text{if } x < 1; \\ 0 & \text{if } x=1. \end{cases} \quad (11)$$

Defining $\kappa_s = \delta_c \rho_{crit} r_s / \Sigma_{cr}$, we can write the convergence as

$$\kappa(x) = \frac{2 \kappa_s}{x^2 - 1} f(x), \quad (12)$$

and the dimensionless mass $m(x)$ as,

$$m(x) = 4 \kappa_s g(x), \quad (13)$$

with

$$g(x) = \ln \frac{x}{2} + \begin{cases} (2/\sqrt{x^2 - 1}) \tan^{-1} \sqrt{(x-1)/(x+1)} & \text{if } x > 1; \\ 2/\sqrt{1-x^2} \tanh^{-1} \sqrt{(1-x)/(1+x)} & \text{if } x < 1; \\ 1 & \text{if } x=1. \end{cases} \quad (14)$$

Equations (10)-(14), together with the algorithm to compute halo parameters outlined by NFW97, can be used to estimate the location of tangential and radial arcs for halos of arbitrary mass.

Finally, we note that the arc thickness is controlled by the angular size of the source and by the value of the convergence at the critical line. As demonstrated by Kovner (1989) and Hammer (1991), the thin dimension of an arc is magnified by a factor of order $\mu \approx 1/2(1 - \kappa)$ relative to its original angular size. Tangential arcs thinner than the source thus require $\kappa(x_t) < 0.5$. We use these results below to analyze the constraints posed by observations of giant arcs on the structure of galaxy clusters.

3. The Dataset

The main properties of clusters in our sample are listed in Table 1. The sample includes all systems in the recent compilation by Wu et al (1998) with measured velocity dispersion. The table lists the following information for each cluster: (1) cluster name, (2) redshift, (3) velocity dispersion in km s^{-1} , (4) designation of the arc used in the analysis (as labeled in the appropriate reference), (5) the redshift of the arc (if available), (6) the arc distance from the center of the cluster, typically chosen to coincide with that of the brightest cluster galaxy, in arcsec, (7) the radial half-light thickness of the arc, in arcsec (upper limits correspond to the seeing of the observation when arc is unresolved), (8) telescope and instrument used, and (9) references for the arc width.

Some values in Table 1 differ from those adopted by Wu et al (1998). **A370:** The giant arc in this strongly bimodal cluster is $10''$ from the nearest bright galaxy and $26''$ from the center of mass of the cluster. As a compromise we take the clustercentric distance of the arc to be $18''$. **AC114:** The most prominent arc, A0, is almost certainly a singly imaged source located beyond the cluster's critical curve. The location of the critical curve is thus not well determined but must lie somewhere inside that radius. There is a multiply imaged system in the same cluster, S1/S2. We estimate the clustercentric distance of the tangential critical line to be the average of A0 and S1/S2, or $38''$. **MS0440:** We take the velocity dispersion of this cluster to be 872 km s^{-1} (Gioia

et al 1998) rather than 606 km s^{-1} (Carlberg et al. 1996), because the former value is more consistent with the cluster’s temperature, $T_X = 5.5 \text{ keV}$, and its (0.1-2.4) keV X-ray luminosity, $L_X = 7.125 \times 10^{43} h^{-2} \text{ erg s}^{-1}$. **C10024**: The redshift of the source galaxy has been determined spectroscopically, $z_s \approx 1.7$ (Broadhurst et al. 1999). **A2124**: Data for this cluster have been taken from Blakeslee & Metzger (1998). **C10016+1609**: Data for this cluster have been taken from Lavery (1996).

The column labeled $\delta\theta_t$ in Table 1 lists the half-light radii of the giant arcs in the radial direction (or the half-seeing if the arc is unresolved). In clusters where more than one tangential arc has width information, the average of the available widths is listed. Except for C10302, where Mathez et al (1992) measure an arc half-width of $0.6''$ for the A1/A1W pair and Luppino et al (1999) quote $< 0.25''$ for the same arc, width estimates from different authors agree to within the errors in all clusters. We take the average of the two discrepant values for C10302.

4. Results

4.1. Main trends in the dataset

Figures 1 and 2 summarize the main trends in the dataset. The top panel in Figure 1 shows the velocity dispersion of the cluster (σ) versus the clustercentric distance of the giant tangential arc (θ_t). Assuming circular symmetry, arc distances can also be expressed in terms of the total projected mass within the arc radius, $M_{core} = \pi \Sigma_{cr} (\theta_t D_l)^2$. This mass estimate depends, through Σ_{cr} and D_l , on the angular diameter distances to source and lens. We have assumed a simple Einstein-de Sitter cosmological model to compute the values of M_{core} plotted in the bottom panel of Figure 1. Arcs without measured redshifts are assumed to be at $z_t = 1$ ³.

The first thing to note from Figure 1 is that core mass and lensing power seem to correlate only weakly with velocity dispersion in clusters with $\sigma \gtrsim 1000 \text{ km s}^{-1}$. This is at odds with scalings expected from simple models. For comparison, the dotted lines in these panels indicate the Einstein radius and the core mass of a singular isothermal sphere at $z_l = 0.3$ lensing a source galaxy located at $z_t = 1.0$ in an Einstein de Sitter universe. The strong dependence on σ expected in this simple model ($M_{core} \propto \sigma^4$) is clearly absent in the data. We note as well that several clusters are more powerful lenses than singular isothermal spheres, indicating a large central concentration of mass in some of these systems.

The filled circles in Figure 2 indicate the (half-light) radial widths of the giant tangential arcs quoted in the literature (see Table 1 for references). Open circles are upper limits to the width derived from the seeing at the time of observation in cases where the arc is unresolved.

³We shall hereafter use subscripts t and r to refer to quantities associated with the source of tangential and radial arcs, respectively.

A clear trend is observed between width and cluster velocity dispersion: arcs become thicker as σ increases. The trend is highly significant. Treating upper limits as measurements, 96.9% of randomly reshuffled $(\sigma, \delta\theta_t)$ samples have a smaller Kendall τ correlation coefficient than the real sample. Neglecting the one deviant point (which corresponds to the arc in Cl0016, deemed unresolved in an HST WFPC2 image by Lavery 1996) increases the significance of the correlation as measured by this test to 99.1%. Because upper limit points are confined exclusively to the low- σ section of the diagram, our procedure most likely underestimates the significance of the correlation.

As discussed in §2.2, the ratio (μ_r) between the radial thickness of tangential arcs and the intrinsic angular extent of the source depends directly on the value of the convergence at the location of the arc, $\mu_r = 1/2[\kappa(x_t) - 1]$. Within this context, the correlation shown in Figure 2 implies that the convergence at the arc location, $\kappa(x_t)$, increases systematically with σ . The actual values of $\kappa(x_t)$ depend on the intrinsic angular size and redshift of the source, which we shall now examine. From Table 1, many of the sources with measured redshifts are at $z_t \sim 0.7$. We compare in Figure 3 their “lensed half-widths” $\delta\theta_t$ with the angular size of field galaxies at various redshifts: (i) the half-light radii of galaxies at intermediate redshifts in the WFPC Medium Deep Survey (Mutz et al 1994), (ii) the half-light radii of $z \sim 1$ galaxies in the CFRS sample of Lilly et al (1998), and (iii) the half-light radii of “Ly-break” galaxies at $z \approx 3$ (starred symbols in Figure 3, from Giavalisco et al 1996).

The data in Figure 3 imply that the angular size of galaxies decreases monotonically out to $z \sim 3$. Taken at face value, intrinsic galaxy sizes also seem to decrease as a function of z , in agreement with predictions from hierarchical models of galaxy formation (Mo, Mao & White 1998). One crude estimate of the evolution may be made by comparing the observational data with the angular extent of a “standard rod” of fixed proper size equal to the average half-light radius of bright ($\sim L_*$) spirals, $\approx 4.4h^{-1}$ kpc (top set of curves, Mutz et al. 1994), and with the angular radius of sources whose proper size scale in inverse proportion to $(1+z)$ (bottom set of lines). The actual evolution in source size out to $z \sim 1$ is approximately intermediate between these two somewhat extreme examples. A word of caution applies to this conclusion. The three surveys shown in Figure 3 have been conducted in different passbands, are subject to different selection biases, and may sample intrinsically different source populations. For example, the Ly-break galaxies seem to be forming stars preferentially in their central regions and therefore would appear substantially smaller in the rest-frame UV used to estimate their sizes than the half-light radii of more passively evolving galaxies examined by the other groups.

With this caveat, we observe that arcs with measured redshifts (filled circles in Figure 3) seem to be of angular size comparable to, or thinner than, field galaxies at similar redshifts. In particular, half-light radii of galaxies in the CFRS survey exceed the arcwidths by about 50%. This may be due in part to the fact that the magnitude-limited CFRS sample is biased towards the bright, large galaxies present at that redshift, while heavily magnified arc sources may be intrinsically fainter and smaller. We conclude, rather conservatively, that the radial magnification

of giant tangential arcs probably does not exceed unity, $\mu_r \lesssim 1$, implying that $\kappa(x_t) \lesssim 0.5$.

4.2. Interpretation of the observed trends

The trends highlighted in Figures 1 and 2 and, in particular, the correlation (or lack thereof) between σ and θ_t suggest that the lensing properties of galaxy clusters differ significantly from those of simple circularly symmetric models such as NFW or the singular isothermal sphere. A number of effects may be responsible for the disagreement; e.g., asphericity in the mass distribution, uncertainties in velocity dispersion estimates, substructure associated with departures from dynamical equilibrium, and the presence of a massive central galaxy.

Let us consider first the effects of asphericity in the mass distribution. N-body models suggest that the distribution of mass in equilibrium galaxy clusters deviates significantly from spherical symmetry, and is well approximated by triaxial shapes maintained by anisotropic velocity dispersion tensors (Thomas et al 1998 and references therein). Estimates of the cluster velocity dispersion and giant arc properties are therefore sensitive to the relative orientation between the principal axes and the line of sight to the cluster. For example, line-of-sight velocity dispersion estimates of cigar-shaped clusters observed end-on would lead to systematic overestimation of the true average σ , but θ_t would be similarly affected by the favorable orientation, in a manner that preserves a firm correlation between σ and θ_t .

Another factor that may affect the observed relation between σ and θ_t are observational uncertainties in σ estimates. Velocity dispersions are notoriously difficult to estimate properly, as the error budget is generally dominated by systematic uncertainties such as cluster membership rather than by strict measurement error (Zabludoff et al 1990, Carlberg et al 1996). The magnitude of the errors required to cause the apparent lack of correlation between σ and θ_t (of order 1000 km s^{-1}) appears, however, excessive. We conclude that projection effects and observational error may contribute significantly to the *scatter* in correlations between lensing and dynamical properties but are unlikely to be the source of the trends shown in Figures 1 and 2.

A simpler alternative is that the projected surface density profile inside θ_t effectively steepens towards lower σ . Indeed, the effective slope of the lensing potential can be deduced in a simple model-independent way, based entirely on observables. Let us approximate the convergence *inside* the tangential arc by a single power law, $\kappa(R) = \kappa_0 R^\alpha$, where κ_0 and α are functions of σ and R is the projected radius. Applying the condition that inside the location of the tangential arc the average value of the convergence is unity, and that the value of $\kappa(R_t)$ at the location of the arc is known from arc's width magnification, we derive the relation $\alpha = 2[\kappa(R_t) - 1]$. In other words, the effective slope of the projected density profile is inversely proportional to the width magnification of the arc. From the data presented in Figures 1 and 2 we see that a $\sigma \sim 1000 \text{ km s}^{-1}$ cluster has $\kappa(R_t) \approx 0.35$ and $\alpha \approx -1.3$. On the other hand, $\sigma_v \gtrsim 1500 \text{ km s}^{-1}$ clusters have much shallower profiles; $\kappa(R_t) \approx 0.6$ and $\alpha \approx -0.8$. *The tangential arc properties of clusters in our sample imply*

that the effective lensing potential is steeper (shallower) than isothermal in $\sigma \lesssim 1250$ ($\sigma \gtrsim 1250$) km s^{-1} clusters. (A singular isothermal sphere has $\alpha = -1$ in this notation.)

As noted in §4.1, the conclusion that the slope of the inner density profile is a strong function of cluster mass is difficult to reconcile with the nearly scalefree structure of cold dark matter halos found in cosmological N-body simulations. This discrepancy afflicts all models where the core structure of dark halos is approximately independent of mass. In particular, slight modifications to the NFW profile that preserve its independence of scale, such as those proposed by Moore et al (1998) and Kravtsov et al (1998), would also fail to reproduce the lensing observations.

We investigate below whether the lensing data may be reconciled with scalefree models such as NFW by assuming that the lensing power of clusters has been significantly boosted by the presence of dynamical substructure and of massive central galaxies, in a way that mimics the correlations between effective slope and σ pointed out above. We emphasize that qualitatively our conclusion applies to all scalefree models of halo structure but we adopt below the NFW description in order to derive *quantitative* estimates of the lensing contribution by the central galaxy and by substructure.

4.3. Comparison with NFW halo models

As discussed in §2, the lensing properties of NFW halos can be computed as a function of velocity dispersion once the lens-source configuration is specified. This allows us to compare the lensing data directly with the predictions of the model. The comparison depends on the values of the cosmological parameters, since these control both the halo parameters (NFW97) and the angular diameter distances of each lens-source configuration. Qualitatively, however, none of the conclusions we discuss below depend on this choice of cosmological model. For illustration, we explore first the lensing properties of NFW clusters in a CDM-dominated universe with $\Omega_0 = 0.2$, $\Lambda = 0.8$, and $h = 0.7$. The power spectrum has been normalized by $\sigma_8 = 1.13$ in order to match the present day abundance of galaxy clusters, as prescribed by Eke, Cole & Frenk (1996). As in Figure 1, we assume that arcs without measured redshift are located at $z_t = 1$.

The top-left panel in Figure 4 shows the ratio between the observed and predicted “Einstein radius” as a function of cluster velocity dispersion. Clearly, CDM halos formed in this cosmology are in general less powerful lenses than actual clusters. This result is not unexpected given our previous discussion: most $\sigma \sim 1000 \text{ km s}^{-1}$ lenses are more powerful than singular isothermal spheres, let alone models with shallower inner density profiles such as NFW. The magnitude of the discrepancy depends strongly on σ . Clusters with $\sigma \sim 1000 \text{ km s}^{-1}$ have Einstein radii about a factor of three larger than expected for NFW models. On the other hand, the light-deflecting power of the most massive clusters in the sample (i.e. those with $\sigma \sim 1500 - 2000 \text{ km s}^{-1}$) agrees well with that of NFW models. (We use for the comparison the halo mean velocity dispersion within the virial radius, $\sigma_{200} = (GM_{200}/2r_{200})^{1/2}$.)

A compounding problem that afflicts cluster mass models with shallow inner density profiles such as NFW was noted by Bartelmann (1996) and concerns the radial magnification of tangential arcs: the convergence at the tangential critical curve is $\kappa(x_t) > 0.5$, implying that the radial magnification exceeds unity. This is shown by the empty circles in the top-left panel of Figure 5. A crude estimate of the “true” radial magnification can be made for arcs with measured redshifts by assuming that the actual source half light radii is $4.4(1 + z_t)^{-1/2} h^{-1}$ kpc (see Figure 3). Values of μ_r computed this way are shown as thick crosses in Figure 5. The difficulty pointed out by Bartelmann (1996) is confirmed by our analysis: observed tangential arcs are roughly 2-3 times thinner than expected from NFW model lenses.

4.4. Dependence on the cosmological parameters

Strictly speaking, the quantitative estimates of the disagreement between NFW models and observations presented above are valid only for the low-density Λ CDM model adopted there, but qualitatively the conclusions are independent of the cosmological parameters. For example, assuming CDM universe models normalized to match the present day abundance of galaxy clusters, we find that changing Ω_0 from 0.2 to 1 (in flat or open geometries) modifies $\theta_t/\theta_{t,pred}$ and μ_r only by about 10-20%, a negligible effect compared to the effects of central galaxy and substructure we explore below.

4.5. The role of substructure

As discussed by Bartelmann, Steinmetz & Weiss (1995), the discrepancy shown in Figure 4 between observed and predicted tangential arc clustercentric distances may be ameliorated by considering the effects of substructure. Let us parameterize this effect by the outward displacement of the tangential arc relative to a circularly averaged NFW halo of the same velocity dispersion, $f_t = \theta_t/\theta_{t,NFW}$. The distribution of f_t has been determined from N-body simulations (Bartelmann & Steinmetz 1996) and is shown by the solid histogram in Figure 6; on average substructure pushes out tangential arcs by 50% in radius. Since there is little indication either from observations or numerical simulations that substructure is a strong function of mass on the scales we probe here, we will assume that all clusters are affected equally, regardless of σ . The upper right panels of Figures 4 and 5 indicate the result of increasing $\theta_{t,pred}$ by $\sim 50\%$ in order to account for this effect. The error bars correspond to the 1/4 and 3/4 quartiles in the distribution of f_t (Figure 6). Note that width magnifications are also reduced because the convergence at the tangential critical curve decreases as the arc moves outwards (Figure 5). Including substructure helps to narrow the gap, but it appears insufficient to reconcile fully the predictions of NFW halo models with observations.

4.6. The effects of a central massive galaxy

The interpretation advanced in §4.2 ascribes the remainder of the difference to the lensing contribution of a central massive galaxy, an ansatz that allows us to estimate its total projected mass within the tangential arc radius. This mass may be compared directly with the stellar mass in the central galaxy, which we estimate as follows. The typical absolute magnitude of brightest cluster galaxies is $M_V - 5 \log h \approx -23.5$ (Schombert 1986), which combined with rough upper limits to the stellar mass-to-light derived from lensing of QSOs by isolated ellipticals, $M/L_V \approx 15hM_\odot/L_\odot$ (Keeton, Kochanek & Falco 1998), imply a total stellar mass of order $M_g \approx 3 \times 10^{11} h^{-1} M_\odot$. Assuming that the galaxy mass profile is well approximated by a de Vaucouleurs law with effective radius, $r_{eff} = 15 h^{-1}$ kpc, we recompute the predicted location of tangential arcs including this contribution and report the results in the bottom-left panels of Figures 4 and 5. The results assume that the structure of the dark halo is modified “adiabatically” by the presence of the central galaxy (see details in NFW96) and are insensitive to our choice of effective radius provided that $r_{eff} \ll \theta_t D_l \approx 60\text{-}120h^{-1}$ kpc; i.e., provided that most of the galaxy’s mass is contained within the tangential critical line. Most brightest cluster galaxies studied so far easily meet this criterion (Schombert 1986).

Predicted arc locations in the bottom-left panel of Figure 4 include the combined effects of substructure and of the stellar component of the central cluster galaxy but are still seen to fall short of observations. This result is rather insensitive to the choice of cosmological model. The disagreement actually grows more acute if higher density universes are considered because Σ_{cr} and, therefore lens masses, increase monotonically with Ω_0 for the lens-source configuration we assume here. Good agreement with observations require that the total mass associated with the central galaxy is increased significantly over and above the expected stellar mass of the galaxy. This is shown in the bottom-right panel of Figures 4 and 5, where we have assumed that the total mass associated with the central galaxy is $M_g = 3 \times 10^{12} h^{-1} M_\odot$, so that the average ratio of θ_t to $\theta_{t,pred}$ is about unity. This galaxy mass corresponds roughly to the mass (projected inside θ_t) of an isothermal sphere with velocity dispersion of order 300 km s⁻¹. This does not seem extravagant: velocity dispersions measured for the central galaxies in MS1358+62, MS2053-04, and MS2124 are all of order ~ 300 km s⁻¹ or higher (Kelson et al 1997, Blakeslee & Metzger 1998), while in cluster RXJ1347.5-1145 the velocity dispersion of stars in the central galaxy is $\sigma = 620$ km s⁻¹ (Sahu et al. 1998).

Reconciling lensing observations with NFW halo models thus require that the central galaxy has somehow managed to retain a sizeable fraction of its own dark halo. This may at first seem puzzling, but is consistent with observational estimates of the mass attached to individual galaxies in clusters. For example, based on the smooth structure of the arc in A370, Kneib et al (1993) conclude that as much as $\sim 10^{11} h^{-1} M_\odot$ may be associated with $M_B - 5 \log(h) \approx -19.6$ galaxies in that cluster. Brightest cluster galaxies are about ~ 30 times more luminous and a simple scaling suggests that halos as massive as $3 \times 10^{12} h^{-1} M_\odot$ may indeed be associated with central cluster galaxies. Our estimate is also consistent with the recent work of Tyson, Fischer & Dell’Antonio

(1999), who argue that mass concentrations surrounding individual galaxies in Cl0024 may be as large as $5 \times 10^{12} h^{-1} M_{\odot}$. A detailed lensing study of A2218 by Kneib et al. (1996) also indicates that individual cluster galaxies with velocity dispersion of order $\sigma = 300 \text{ km s}^{-1}$ must be surrounded with halos of mass $\sim 10^{12} h^{-1} M_{\odot}$. We note as well that the total mass associated with the central galaxy would actually be lower if, as proposed by Moore et al (1998), our procedure had somehow underestimated the central density concentration of the cluster halo. These authors report that NFW concentration parameter obtained from the procedure outlined in NFW97 may be as much as 50% lower than required to fit their numerical experiments. Our conclusion does not change qualitatively, but the mass of the central galaxy in this case would need to be revised downward by approximately 50% in order to fit the data.

5. Implications of the model

5.1. Radial Arcs

Our conclusion that the mass associated with the luminous central galaxy plays a fundamental role in the lensing properties of the cores of galaxy clusters can be tested directly by considering the formation of radial arcs. These arcs are located at the radial critical lines, x_r , where the eigenvalue λ_r vanishes. We see from eqs. 8 and 9 that the location of the radial arc depends on the angular gradient of the projected mass, rather than on the mean enclosed surface density. Their location, therefore, may in principle be used to verify independently our conclusion that the surface density profile steepens systematically towards decreasing σ .

In the absence of a massive central galaxy, the relative location of radial and tangential arcs formed through lensing by NFW halos is straightforward to compute once the angular diameter distances to the sources are known. Conversely, knowledge of the relative location of the arcs and of the tangential arc redshift uniquely determines the redshift of the radial arc. For example, Bartelmann (1996) applies this procedure to the radial/tangential arc system in MS2137 and concludes that the sources of both arcs must be either at very similar redshifts, or else far behind the cluster at $z \gg 1$. The dichotomy simply reflects the fact that neither arc has measured redshift. The tangential arc redshift is known for A370 (Soucail et al 1988), and the same analysis yields a prediction $z_r \sim 1.5$ for the radial arc, in reasonable agreement with the $z_r \approx 1.3$ prediction from the detailed lens models of Kneib et al (1993) and Smail et al (1995). Radial arcs have now been observed in four clusters: MS0440, MS2137, A370, and AC114. These clusters span the entire range in velocity dispersion of our sample (AC114 has one of the highest velocity dispersions, $\sigma = 1649 \text{ km s}^{-1}$, and MS0440 has one of the lowest, $\sigma = 872 \text{ km s}^{-1}$), and therefore we expect that the systematic trends inferred in the previous subsection may have a detectable influence on the properties of the radial arcs.

One simple trend predicted by our interpretation concerns the relative location of radial and tangential arcs as a function of the cluster velocity dispersion. Assuming that the sources are at

similar redshifts, the ratio between the clustercentric distances of radial and tangential arcs, θ_r/θ_t , depends strongly on the slope of the surface density profile inside θ_t : the steeper the profile the closer to the center the radial arc moves and the smaller θ_r/θ_t becomes. This is shown in Figure 7, where the open circles represent the predictions of our model for all clusters in our sample (including the effect of a central galaxy of mass $M_g = 3 \times 10^{12} h^{-1} M_\odot$). We assume that the redshifts of both arcs are the same, $z_r = z_t$, and adopt the same fiducial cosmology of Figures 4 and 5. The arcs in MS0440, MS2137 and AC114 follow the predicted trend very well, but the radial arc in A370 is much farther than expected in our simple model. This may be because the source of the radial arc is much farther behind the cluster than the tangential arc source; $z_r \approx 2z_t \sim 1.4$, again in good agreement with the predictions of Smail et al (1995).

In summary, the relative location of radial and tangential arcs is a useful test of the conclusions reached in the previous subsection regarding the role played by the central galaxy on the lensing properties of clusters. Although there are no measured redshifts for radial arcs, our analysis predicts that the arc sources in MS0440, MS2137, and AC114 are at very similar redshifts. Consistency with our model requires that the radial arc source must be far behind the tangential arc in A370. Spectroscopic redshifts of radial arcs may thus be used to verify or rule out the applicability to actual clusters of the mass modeling we propose here.

5.2. Observability of lensed features

A second corollary of the interpretation outlined in §4.2 is that, because lensing features depend so heavily on the mass of the central galaxy, at fixed cluster velocity dispersion tangential arc distances must correlate with the total luminosity of the central galaxy. This could in principle be demonstrated by comparing the residuals of the σ - θ_t correlation shown in Figure 1 with residuals of the correlation between σ and the total luminosity of the central galaxy. A search of the literature yields, unfortunately, few total absolute magnitudes for brightest cluster galaxies in our sample, and therefore we are unable to utilize this test to verify our interpretation. We intend to use archival images of clusters from different telescopes and revisit this question in a future paper.

We note here that, if our interpretation is correct, it would help to explain the apparent underrepresentation of moderate- σ clusters in current lensing samples. Estimates based on the Press-Schechter (1974) algorithm predict that clusters with $\sigma \gtrsim 1000 \text{ km s}^{-1}$ should outnumber clusters with $\sigma \gtrsim 1500 \text{ km s}^{-1}$ by a factor of ~ 20 or more (Eke et al 1998), a result of the exponential decline of the cluster mass function at the high-mass end. This sharp decrease in the number of clusters with increasing σ is not readily apparent in lensing samples. For example, in the sample compiled here $\sigma \gtrsim 1000 \text{ km s}^{-1}$ are only about twice as numerous as $\sigma \gtrsim 1500 \text{ km s}^{-1}$ systems, suggesting the operation of a mechanism that hinders the observability of lensed features in low- σ clusters. Our discussion above hints at one possibility: out of all low-mass clusters only those with very massive central galaxies may display easily identifiable lensed features.

In these systems, tangential arcs are long and thin and appear at large distances from the center, thereby increasing their visibility to surveys looking preferentially for images with large length-to-width ratio. Without massive central galaxies the lensing power of low-mass clusters would be substantially reduced; arcs would occur closer to the center (where they are hard to distinguish from a central galaxy), would be significantly magnified in both radial and tangential directions (see Figure 5 and the discussion by Williams & Lewis 1998), and may thus readily have escaped detection as “giant arcs”.

6. Summary

We compare the lensing properties of galaxy clusters with the predictions of cluster models based on the NFW density profile. We find that clusters are in general more powerful lenses than NFW halos of similar velocity dispersion. The magnitude of the discrepancy is small for the most massive clusters in our sample, $\sigma \sim 1500 - 2000 \text{ km s}^{-1}$, but increases towards lower cluster velocity dispersions. NFW lenses also yield large radial magnifications at the tangential arc location, at odds with observations which indicate that tangential arc widths are of order of (or perhaps thinner than) the typical angular size of possible galaxy sources. We use a simple analysis to show that the data are best reproduced by mass models where the inner slope of the projected cluster density profile steepens significantly with decreasing σ . Agreement with the data requires the effective core lensing potential to be steeper than isothermal in $\sigma \sim 1000 \text{ km s}^{-1}$ clusters, but shallower than isothermal in the most massive clusters in the sample ($\sigma \sim 1500\text{-}2000 \text{ km s}^{-1}$).

We interpret the disagreement between NFW models and lensing observations as signaling the contribution to the cluster lensing potential of significant amounts of substructure and of massive central galaxies. Provided that central galaxy mass correlates only weakly with σ , its contribution to lensing is more important in less massive clusters, reproducing the observed trends. We use N-body simulations to calibrate the effects of substructure, and estimate that central galaxies as massive as $M_g \approx 3 \times 10^{12} h^{-1} M_\odot$ are needed to reconcile NFW halo models with observations. This is much larger than estimates of the stellar mass of the galaxy; agreement between lensing data and NFW halo models requires that the central galaxy be surrounded by a dark matter halo which, within the arc radius, contains almost ten times as much mass as associated with stars. Lower galaxy masses may be acceptable if, as suggested by recent N-body experiments, the NFW model systematically underestimates the central concentration of dark matter halos (Moore et al 1998).

Qualitatively, this conclusion applies to all dark halo models where the inner slope within the Einstein radius is approximately independent of mass, although the quantitative estimates presented above are strictly valid only for NFW models and for the Λ CDM model we explore. Quantitative estimates, however, are quite insensitive to the values of the cosmological parameters, varying only by 10-20% when Ω_0 is allowed to vary between 0.2 and 1 (in open and flat geometries).

A crucial ingredient of this interpretation is that the less massive the cluster the more conspicuous the lensing role played by the central galaxy. The role of a central galaxy in modifying the cluster's inner profile can in principle be tested through observations of radial/tangential arc systems. Our modeling predicts that the redshifts of the radial and tangential arcs must be similar in MS0440, MS2137, and AC114, but that the radial arc source is far behind the tangential arc source in A370. Radial arc redshifts are therefore sensitive tests of our model predictions. These observations are within reach of the 8-10m class telescopes coming into operation, so we should be able to assess the validity of the modeling we propose here very soon indeed.

This work has been supported in part by the National Science and Engineering Research Council of Canada. JFN acknowledges useful discussions with Mike Hudson, Greg Fahlman, and Ian Smail.

Table 1: Tangential Arcs in Clusters

Cluster	z_l	σ_v [km/s]	Arc	z_s	θ [asec]	$\delta\theta_t$ [asec]	Telescope	References
A370	0.373	1367	A0	0.724	10	0.54	WFC1	1, 2, 3, 4, 5
A963	0.206	1100		0.711	18.5	<0.50	UH 2.2m	1, 6
A1689	0.181	1989		-	46.5	-	-	1
A2124	0.066	878		0.573	27	0.30	KeckII	7
A2163	0.203	1680		0.728	15.5	-	-	1
A2218	0.171	1405	#359	0.702	21.2	0.47	WFPC2	1, 5, 8, 9
A2280	0.326	948		-	13.9	<0.45	UH 2.2m	1, 10
A2390	0.228	1093	H1	0.913	38	0.65	CFHT	1, 11, 12, 13
A2744	0.308	1950		-	21.4	-	-	1
S295	0.299	907		0.93	25.5	<0.57	ESO 3.6m	1, 14
MS0440+0204	0.197	872	2	0.53	21.8	0.40	UH, CFHT	1, 15, 16, 17
			3	"	22.8	<0.25	"	"
MS0451-0305	0.539	1371	A1	-	32	0.45	UH, CFHT	1, 16
			A2	-	22	0.45	"	"
MS1006+1201	0.221	906	A2	-	27	0.60	UH, CFHT	1, 16, 18
			A3	-	18	0.40	"	"
MS1008-1224	0.306	1054	1	-	45	0.40	UH, CFHT	1, 16, 18
			2	-	53	0.30	"	"
MS1358+6245	0.329	987		4.92	23	<0.40	UH, CFHT	1, 16, 19
MS1455+2232	0.257	1133	1	-	21	0.65	UH, CFHT	1, 16, 18
AC114	0.310	1649	A0	0.639	62.4	0.78	WFC1	1, 5, 20
			S1/S2	-	13.5	0.63	"	1, 5, 21
Cl0016+1609	0.545	1234	1	-	25	<0.10	WFPC2	22
Cl0024+1654	0.391	1339	C	1.7	34.6	0.78	WFC1	1, 5, 23, 24
Cl0302+1658	0.423	1100	A1/A1W	0.8	18.5	0.6	CFHT	1, 25
			A1/A1W	-	18	<0.25	UH, CFHT	1, 16
Cl0500-24	0.327	1152		-	25.9	-	-	1, 26
MS1621+2640	0.427	793	A1	-	6.9	<0.25	-	1, 16, 27
MS2137-2353	0.313	960	A0	-	15.5	0.40	ESO NTT	1, 28
RX1347-1145	0.451	1235	1	-	34.2	0.38	STIS	1, 29, 30
			4	-	36.3	0.25	"	"

¹ Wu et al (1998); ² Soucail et al (1987a); ³ Soucail et al (1987b); ⁴ Soucail et al (1988); ⁵ Smail et al (1996); ⁶ Lavery & Henry (1988); ⁷ Blakeslee et al (1999); ⁸ Le Borgne et al (1992); ⁹ Pello et al (1992); ¹⁰ Gioia et al (1995); ¹¹ Pello et al (1991); ¹² Le Borgne et al (1991); ¹³ Mellier (1989); ¹⁴ Edge et al (1994); ¹⁵ Gioia et al (1998); ¹⁶ Luppino et al (1999); ¹⁷ Luppino et al (1993); ¹⁸ Le Fevre et al (1994) ¹⁹ Luppino et al (1991); ²⁰ Smail et al (1991); ²¹ Smail et al (1995); ²² Lavery (1996); ²³ Colley et al (1996); ²⁴ Koo (1988); ²⁵ Mathez et al (1992); ²⁶ Giraud (1988); ²⁷ Luppino & Gioia (1992); ²⁸ Fort et al (1992); ²⁹ Sahu et al (1998); ³⁰ Schindler et al (1995)

REFERENCES

- AbdelSalam, H.M., Saha, P. & Williams, L.L.R. 1998, *AJ*, 116, 1541
- Bartelmann, M. 1996, *A&A*, 313, 697
- Bartelmann, M. & Steinmetz, M. 1996, *MNRAS*, 283, 431
- Bartelmann, M., Steinmetz, M. & Weiss, A. 1995, *A&A*, 297, 1
- Blakeslee, J.P. & Metzger, M.R. 1999, *ApJ*, 513, 592
- Blandford, R.D. & Narayan, R. 1992, *ARA&A*, 30, 311
- Broadhurst, T., Huang, X., Frye, B. & Ellis, R.S. 1999, astro-ph/9902316
- Carlberg, R.G., Yee, H.K.C., Ellingson, E., Abraham, R., Gravel, P., Morris, S. & Pritchet, C.J. 1996, *ApJ*, 462, 32
- Colley, W.N., Tyson, J.A. & Turner, E.L. 1996, *ApJ*, 461, L86
- Edge, A.C., Boehringer, H., Guzzo., L. et al. 1994, *A&A*, 289, L34
- Eke, V.R., Cole, S. & Frenk, C.S. 1996, *MNRAS*, 282, 263
- Fort, B., Le Fevre, O., Hammer, F. & Cailloux, M. 1992, *ApJ*, 399, L125
- Giavalisco, M., Steidel, C.C. & Macchetto, F.D. 1996, *ApJ*, 470, 189
- Gioia, I.M., Henry, J.P., Luppino, G.A., Clowe, D.I., Boehringer, H., Briel, U.G. Voges, W., Huchram J.P. & MacGillivray, H. 1995, *A&A*, 297, L75
- Giraud, E. 1988, *ApJ*, 334, L69
- Gioia, I.M., Shaya, E.J., Le Fevre, O., Falco, E.E., Luppino, G.A. & Hammer, F. 1998, *ApJ*, 497, 573
- Hammer, F. 1991, *ApJ*, 383, 66
- Keeton, C.R., Kochanek, C.S. & Falco, E.E. 1999, *ApJ*, 509, 561
- Kelson, D.D., van Dokkum, P.G., Franx, M., Illingworth, G.D. & Fabricant, D. 1997, *ApJ*, 478, L13
- Kneib, J.-P., Ellis, R.S., Smail, I., Couch, W.J., Sharples, R.M. 1996, *ApJ*, 471, 643
- Kneib, J.-P., Mellier, Y., Fort, B. & Mathez, G. 1993, *A&A*, 273, 367
- Koo, D. C. 1988, in *Large-Scale Motions in the Universe*, ed. V. C. Rubin & G. V. Coyne (Princeton: Princeton Univ. Press), 513

- Kovner, I. 1989, *ApJ*, 337, 621
- Kravtsov, A.V., Klypin, A.A., Bullock, J.S. & Primack, J.R. 1998, *ApJ*, 502, 48
- Lavery, R.J. 1996, *AJ*, 112, 1812
- Lavery, R.J. & Henry, J.P. 1988, *ApJ*, 329, L21
- Le Borgne, J.-F., Pello, R. & Sanahuja, B. 1992, *A&AS*, 95, 87
- Le Borgne, J.-F., Mathez, G., Mellier, Y., Pello, R., Sanahuja, B. & Soucail, G. 1991, *A&AS*, 88, 133
- Le Fevre, O., Hammer, F., Angonin, M.C., Gioia, I.M. & Luppino, G.A. 1994, *ApJ*, 422, L5
- Lilly, S., Schade, D., Ellis, R. et al 1998, *ApJ*, 500, 75
- Luppino, G.A. & Gioia, I.M. 1992, *A&A*, 265, L9
- Luppino, G.A., Gioia, I.M., Hammer, F., Le Fevre, O. & Annis, J.A. 1999, *A&AS*, 136, 117
- Luppino, G.A., Gioia, I.M., Annis, J.A., Le Fevre, O. & Hammer, F. 1993, *ApJ*, 416, 444
- Luppino, G.A., Cooke, B.A., McHardy, I.M. & Ricker, G.R. 1991, *AJ*, 102, 1
- Lynds, R. & Petrosian, V. 1986, *Bull.AAS*, 18, 1014
- Mathez, G., Fort, B., Mellier, Y., Picat, J.-P. & Soucail, G. 1992, *A&A*, 256, 343
- Mellier, Y. 1989, in *Proc. of the Space Telescope Science Institute on ‘Clusters of Galaxies’*, Baltimore, MD, ed. M. Fitchett
- Mo, H.J., Mao, S. & White, S.D.M. 1998, *MNRAS*, 295, 319
- Moore, B., Governato, F., Quinn, T., Stadel, J. & Lake, G. 1998, *ApJ*, 499, L5
- Mutz, S.B., Windhorst, R.A., Schmidtke, P.C., et al. 1994, *ApJ*, 434, 55
- Narayan, R. & Bartelmann, M. 1996, *astro-ph/9606001*
- Narayan, R., Blandford, R. & Nityananda, R. 1984, *Nature*, 310, 112
- Navarro, J.F., Frenk, C.S. & White, S.D.M. 1996, *ApJ*, 462, 563
- Navarro, J.F., Frenk, C.S. & White, S.D.M. 1997, *ApJ*, 490, 493
- Pello, R., Le Borgne, J.-F., Sanahuja, B., Mathez, G. & Fort, B. 1992, *A&A*, 266, 6
- Pello, R., Le Borgne, J.-F. Soucail, G., Mellier, Y. & Sanahuja, B. 1991, *ApJ*, 366, 405

- Sahu, K.C., Shaw, R.A., Kaiser, M.E. et al 1998, ApJ, 492, L125
- Schindler, S., Guzzo, L., Ebeling, H. et al. 1995, A&A, 299, L9
- Schneider, P., Ehlers, J. & Falco, E.E. 1992, Gravitational Lenses (Heidelberg: Springer)
- Schombert, J.M. 1986, ApJS, 60, 603
- Soucail, G., Mellier, Y., Fort, B., Mathez, G. & Cailloux, M. 1988, A&A, 191, L19
- Soucail, G., Mellier, Y., Fort, B., Hammer, F. & Mathez, G. 1987b, A&A, 184, L7
- Soucail, G., Fort, B., Mellier, Y., & Picat, J.P. 1987a, A&A, 172, L14
- Smail, I., Couch, W.J., Ellis, R.S. & Sharples, R.M. 1995, ApJ, 440, 501
- Smail, I., Dressler, A., Kneib, J.-P., Ellis, R.S., Couch, W.J., Sharples, R.M. & Oemler, A. 1996, ApJ, 469, 508
- Smail, I., Ellis, R.S., Fitchett, M.J., Norgaard-Nielsen, H.U., Hansen, L. & Jorgensen, H.E. 1991, MNRAS, 252, 19
- Press, W.H. & Schechter, P. 1974, ApJ, 187, 425
- Thomas, P.A., Colberg, J.M., Couchman, H.M.P., Efstathiou, G.P.; Frenk, C.S., Jenkins, A.R., Nelson, A.H., Hutchings, R.M., Peacock, J.A., Pearce, F.R., White, S.D.M. 1998, MNRAS 296, 1061.
- Williams, L.L.R. & Lewis, G.F. 1998, MNRAS, 294, 299
- Wu, X.-P., Chiueh, T., Fang, L.-Z. & Xue, Y.-J. 1998, MNRAS, 301, 861
- Zabludoff, A.I., Huchra, J.P. & Geller, M.J. 1990, ApJS, 74, 1

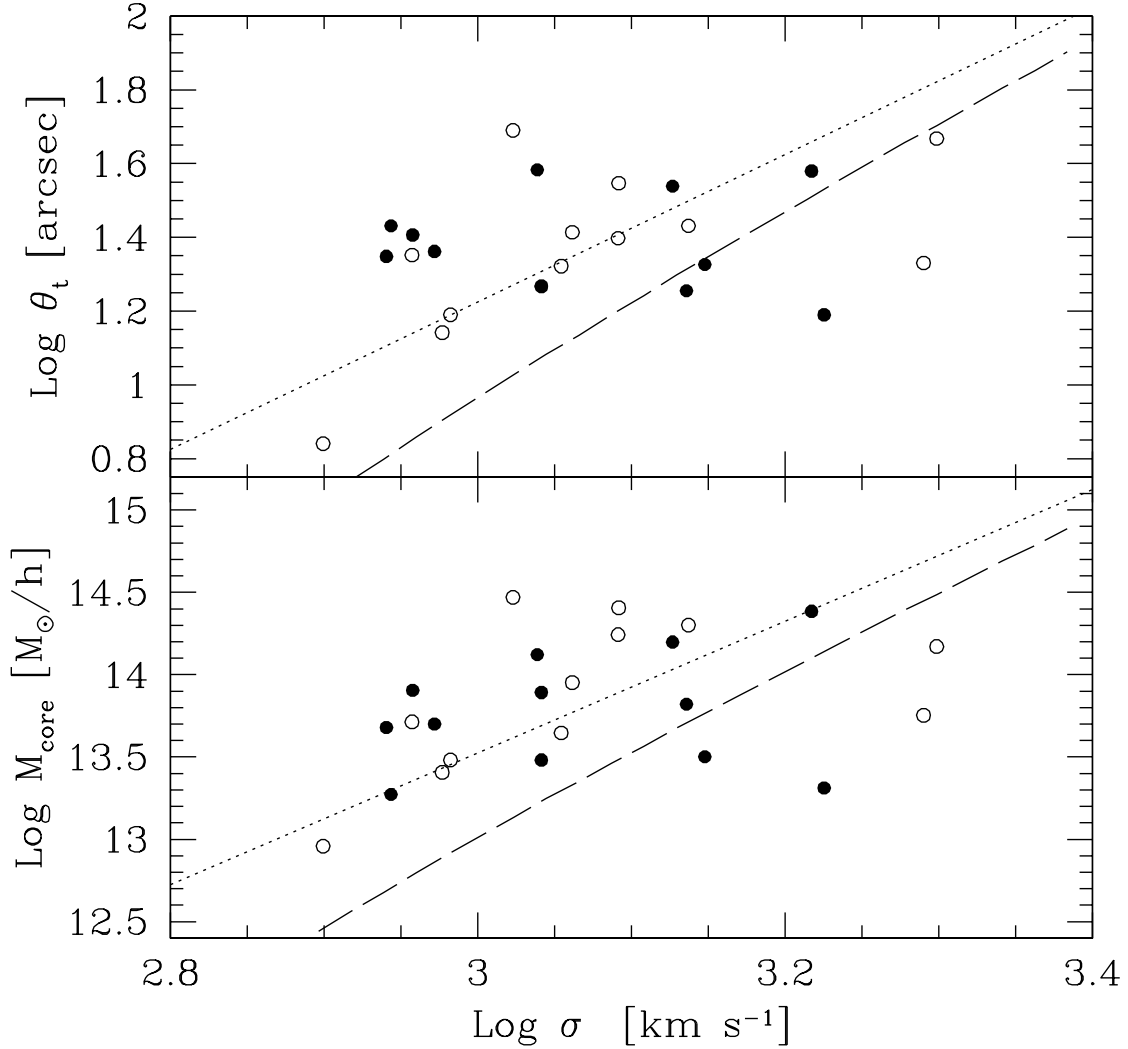


Fig. 1.— The strong lensing properties of galaxy clusters in our sample as a function of cluster velocity dispersion, σ . Arcs without spectroscopic redshifts are assumed to be at $z_s \sim 1$, and are marked by empty circles. The dotted and dashed lines are for singular isothermal sphere and NFW cluster models, respectively, assuming that clusters are located at $z_l = 0.3$ and that the sources are at $z_s = 1$. *Top panel:* clustercentric distance of the tangential arc (the “Einstein radius”) in arcsec. *Bottom panel:* cluster core mass derived from the top panel assuming circular symmetry and angular diameter distances appropriate to an Einstein-de Sitter universe.

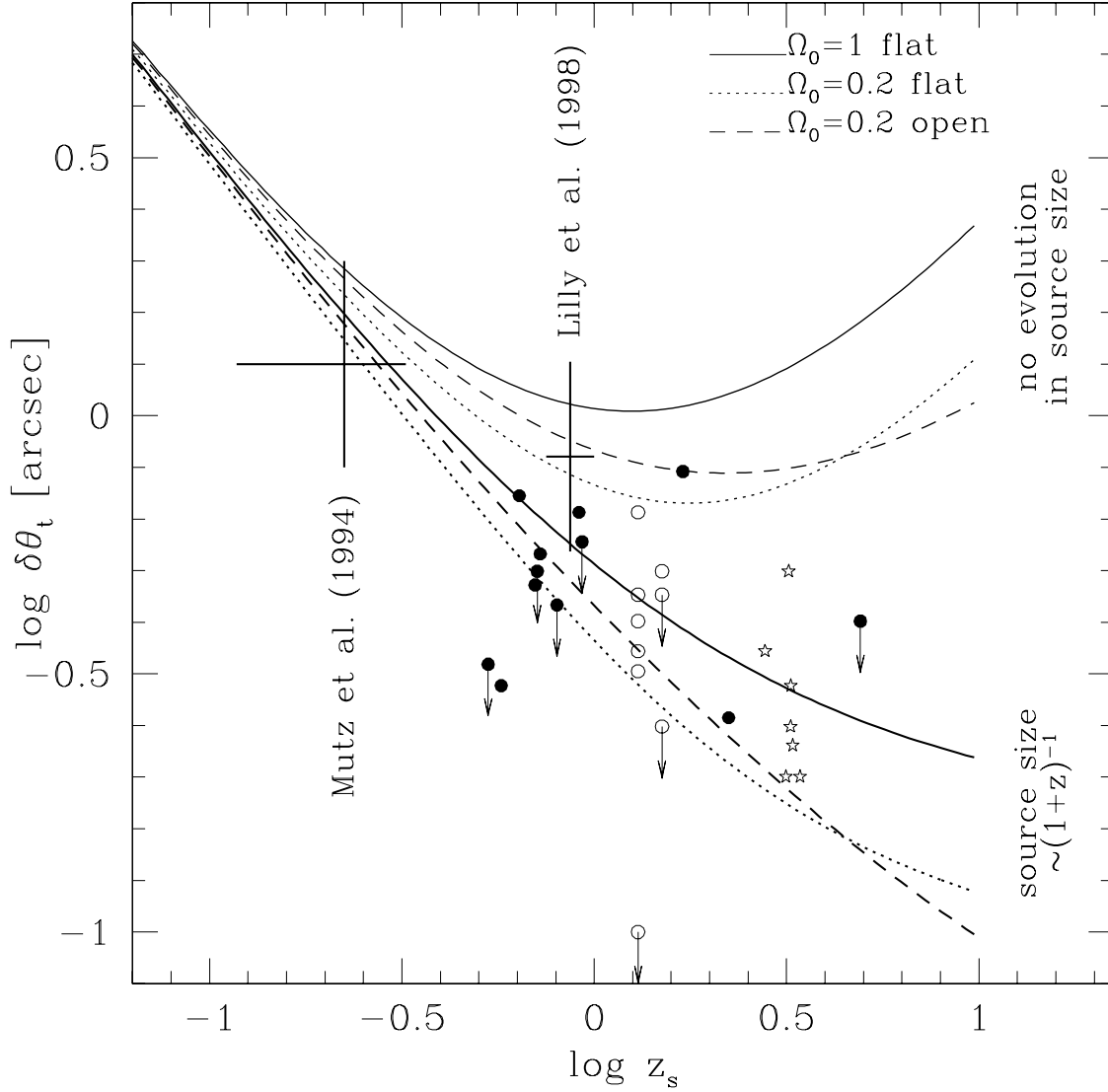


Fig. 3.— The tangential arc half-widths (filled circles) compared with the intrinsic angular size of galaxies at different redshifts from the HST MDS survey of Mutz et al (1994), the CFRS survey of Lilly et al (1998), and the Ly-break galaxies of Giavalisco et al (1996) (starred symbols). Arcs without redshifts are shown with open circles. Note that arc widths are comparable (or smaller) than the angular size of galaxies at comparable redshifts, indicating that the radial magnification at the tangential critical line is about (or less than) unity.

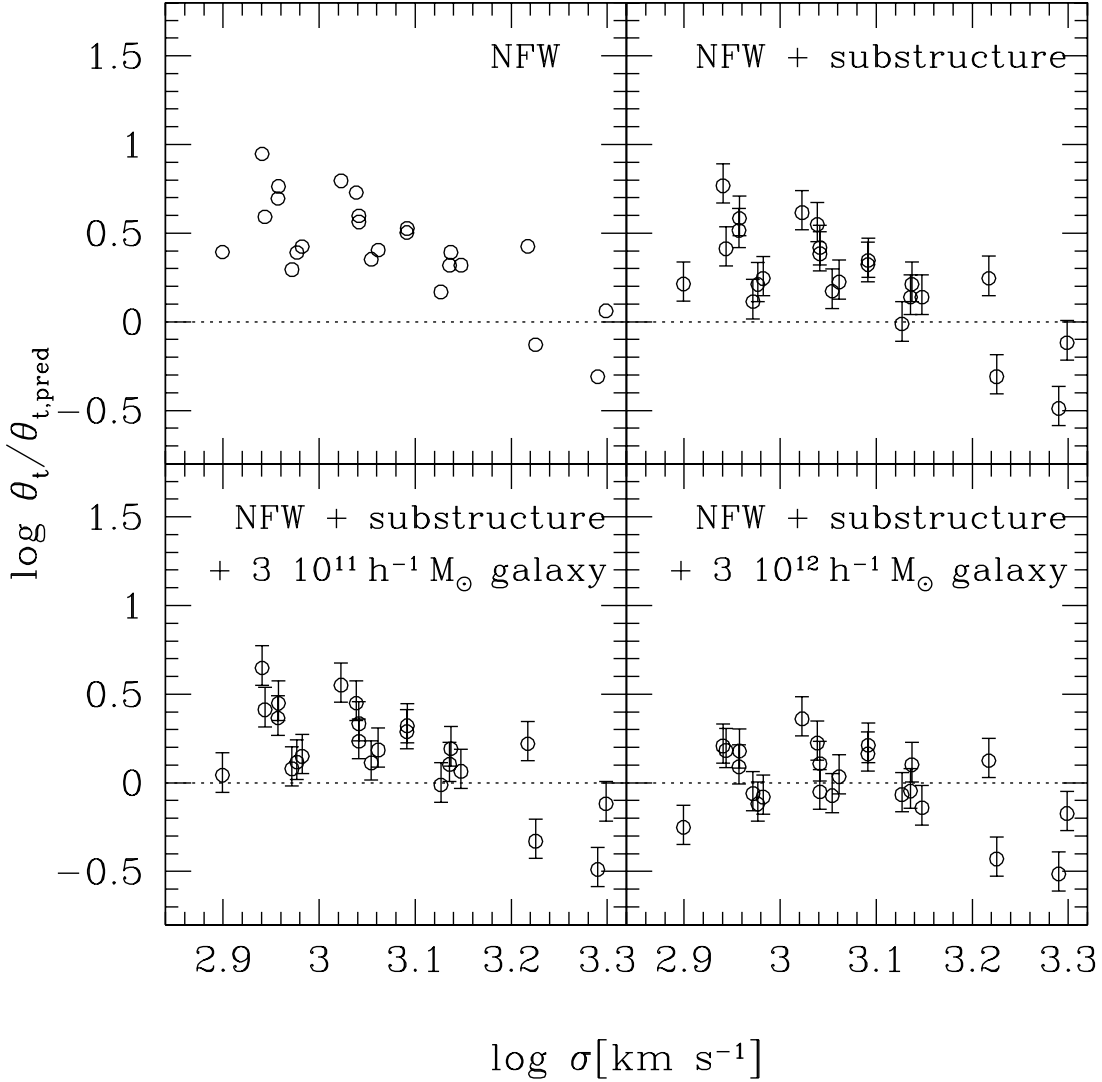


Fig. 4.— *Top left:* Ratio between the observed clustercentric distance of tangential arcs and the predictions of NFW halo models in an $\Omega_0 = 0.2$, $\Lambda = 0.8$, $h = 0.7$ cluster-normalized cold dark matter dominated universe. *Top right:* as in top left panel, but assuming that the lensing properties of NFW halos are aided by substructure as described in §4.4. The error bars represent the 1/4 and 3/4 quartile range of the substructure f_t parameter, see Figure 6. *Bottom left:* as in top left panel, but assuming that the lensing properties of NFW halos are aided by the presence of substructure and a central galaxy with $M_g = 3 \times 10^{11} h^{-1} M_\odot$, see §4.5. *Bottom right:* as in bottom left, but with $M_g = 3 \times 10^{12} h^{-1} M_\odot$.

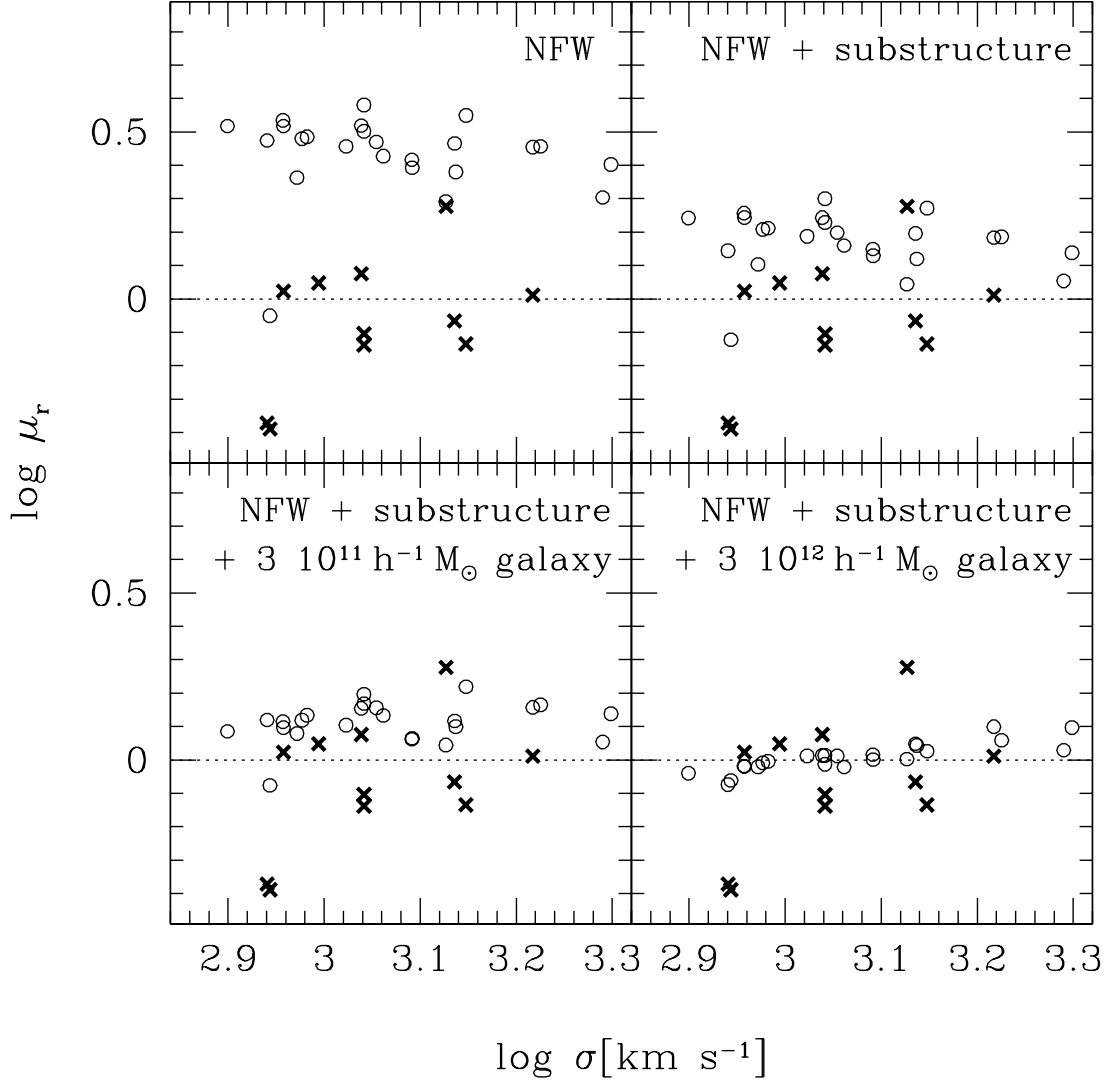


Fig. 5.— Panels are as in Figure 4, but for the radial magnification at the tangential critical line, $\mu_r(\theta_t)$ (empty circles). Crosses indicate magnification estimates based on observed arc widths and redshifts, and the assumption that the intrinsic angular size of the source is $4.4(1+z_s)^{-1/2} h^{-1}$ kpc.

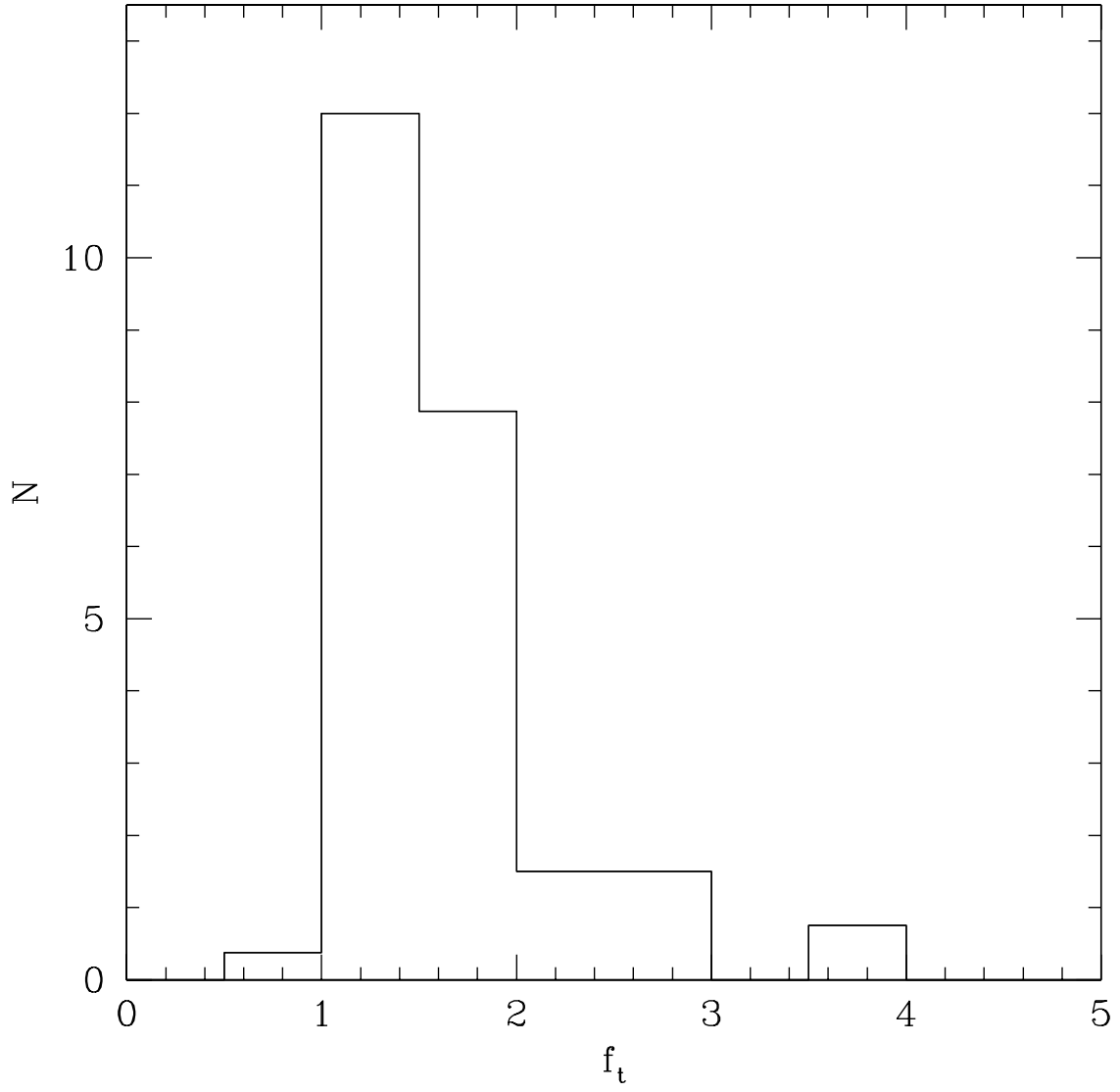


Fig. 6.— The distribution of substructure parameter, f_t , obtained from N-body simulations and used to estimate “uncertainties” in Figures 4 and 5.

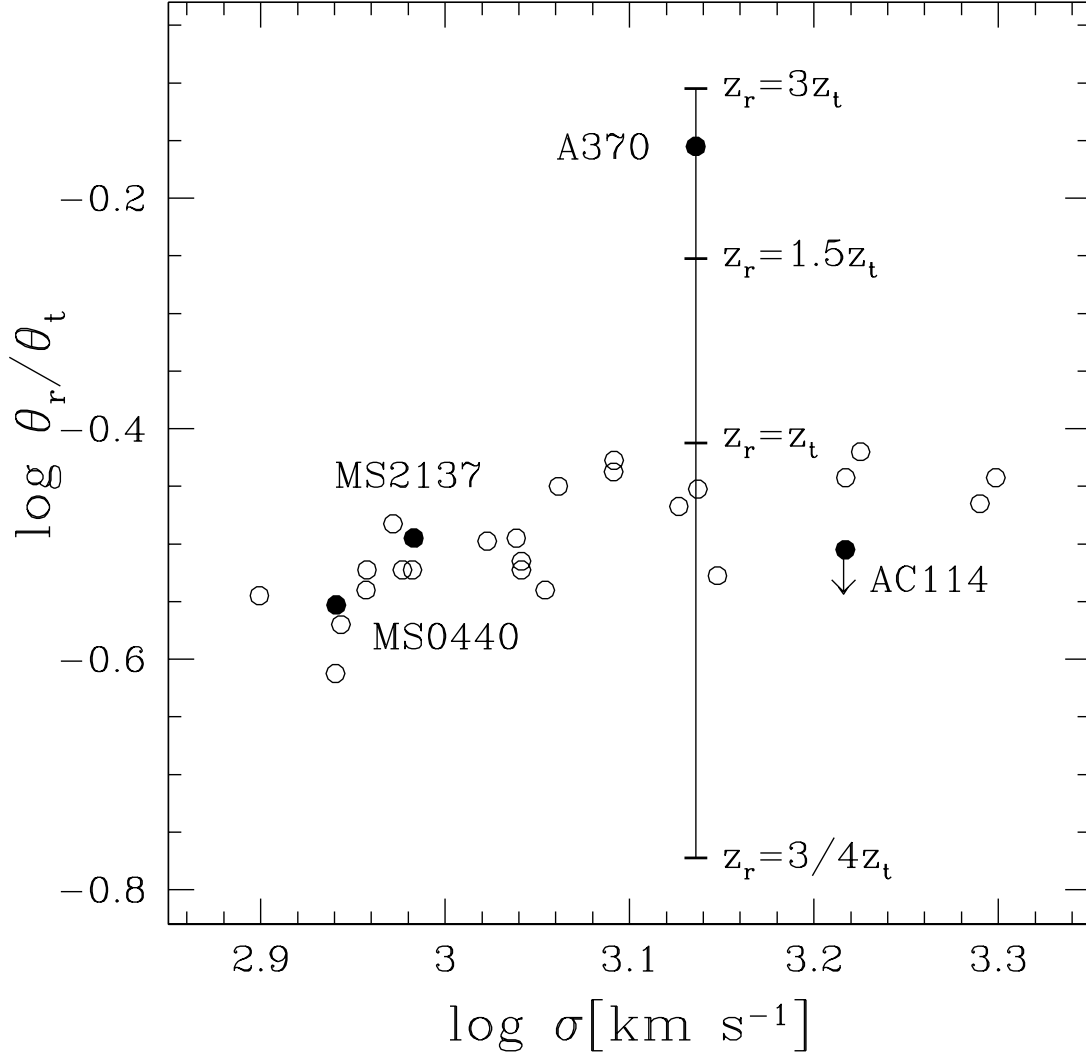


Fig. 7.— The ratio between clustercentric distance of radial and tangential arcs for NFW cluster models that include a $M_g = 3 \times 10^{11} h^{-1} M_\odot$ central galaxy, as described in §4.5. Open circles are the model predictions as a function of cluster velocity dispersion, assuming that both arcs are at the same redshift. Tangential arc redshifts are assumed to be $z_s = 1$ if unavailable. Data for MS0440, MS2137 and AC114 are consistent with this assumption, but A370 deviates strongly from the predicted trend. This may indicate that the radial arc source is far behind the tangential arc galaxy, at $z_r \approx 2-3 z_t$. A spectroscopic redshift determination of this arc would be useful for assessing the validity of our mass model.